

Investigation of the linear and mode-coupled flow harmonics in Au+Au collisions at $\sqrt{s_{NN}}=200$ GeV

J. Adam⁶, L. Adamczyk², J. R. Adams³⁹, J. K. Adkins³⁰, G. Agakishiev²⁸,
M. M. Aggarwal⁴¹, Z. Ahammed⁶¹, I. Alekseev^{3,35}, D. M. Anderson⁵⁵, A. Aparin²⁸,
E. C. Aschenauer⁶, M. U. Ashraf¹¹, F. G. Atetalla²⁹, A. Attri⁴¹, G. S. Averichev²⁸,
V. Bairathi⁵³, K. Barish¹⁰, A. Behera⁵², R. Bellwied²⁰, A. Bhasin²⁷, J. Bielcik¹⁴,
J. Bielcikova³⁸, L. C. Bland⁶, I. G. Bordyuzhin³, J. D. Brandenburg^{6,49},
A. V. Brandin³⁵, J. Butterworth⁴⁵, H. Caines⁶⁴, M. Calderón de la Barca Sánchez⁸,
D. Cebra⁸, I. Chakaberia^{29,6}, P. Chaloupka¹⁴, B. K. Chan⁹, F-H. Chang³⁷, Z. Chang⁶,
N. Chankova-Bunzarova²⁸, A. Chatterjee¹¹, D. Chen¹⁰, J. H. Chen¹⁸, X. Chen⁴⁸,
Z. Chen⁴⁹, J. Cheng⁵⁷, M. Cherney¹³, M. Chevalier¹⁰, S. Choudhury¹⁸, W. Christie⁶,
X. Chu⁶, H. J. Crawford⁷, M. Csanád¹⁶, M. Daugherty¹, T. G. Dedovich²⁸,
I. M. Deppner¹⁹, A. A. Derevschikov⁴³, L. Didenko⁶, X. Dong³¹, J. L. Drachenberg¹,
J. C. Dunlop⁶, T. Edmonds⁴⁴, N. Elsey⁶³, J. Engelage⁷, G. Eppley⁴⁵, R. Esha⁵²,
S. Esumi⁵⁸, O. Evdokimov¹², A. Ewigleben³², O. Eyser⁶, R. Fatemi³⁰, S. Fazio⁶,
P. Federic³⁸, J. Fedorisin²⁸, C. J. Feng³⁷, Y. Feng⁴⁴, P. Filip²⁸, E. Finch⁵¹, Y. Fisyak⁶,
A. Francisco⁶⁴, L. Fulek², C. A. Gagliardi⁵⁵, T. Galatyuk¹⁵, F. Geurts⁴⁵, A. Gibson⁶⁰,
K. Gopal²³, D. Grosnick⁶⁰, W. Guryon⁶, A. I. Hamad²⁹, A. Hamed⁵, S. Harabasz¹⁵,
J. W. Harris⁶⁴, S. He¹¹, W. He¹⁸, X. H. He²⁶, S. Heppelmann⁸, S. Heppelmann⁴²,
N. Herrmann¹⁹, E. Hoffman²⁰, L. Holub¹⁴, Y. Hong³¹, S. Horvat⁶⁴, Y. Hu¹⁸,
H. Z. Huang⁹, S. L. Huang⁵², T. Huang³⁷, X. Huang⁵⁷, T. J. Humanic³⁹, P. Huo⁵²,
G. Igo⁹, D. Isenhower¹, W. W. Jacobs²⁵, C. Jena²³, A. Jentsch⁶, Y. Ji⁴⁸, J. Jia^{6,52},
K. Jiang⁴⁸, S. Jowzaee⁶³, X. Ju⁴⁸, E. G. Judd⁷, S. Kabana⁵³, M. L. Kabir¹⁰,
S. Kagamaster³², D. Kalinkin²⁵, K. Kang⁵⁷, D. Kapukchyan¹⁰, K. Kauder⁶, H. W. Ke⁶,
D. Keane²⁹, A. Kechechyan²⁸, M. Kelsey³¹, Y. V. Khyzhniak³⁵, D. P. Kikoła⁶²,
C. Kim¹⁰, B. Kimelman⁸, D. Kincses¹⁶, T. A. Kinghorn⁸, I. Kisel¹⁷, A. Kiselev⁶,
M. Kocan¹⁴, L. Kochenda³⁵, L. K. Kosarzewski¹⁴, L. Kramerik¹⁴, P. Kravtsov³⁵,
K. Krueger⁴, N. Kulathunga Mudiyansele²⁰, L. Kumar⁴¹,
R. Kunnawalkam Elayavalli⁶³, J. H. Kwasizur²⁵, R. Lacey⁵², S. Lan¹¹, J. M. Landgraf⁶,
J. Lauret⁶, A. Lebedev⁶, R. Lednicky²⁸, J. H. Lee⁶, Y. H. Leung³¹, C. Li⁴⁸, W. Li⁵⁰,
W. Li⁴⁵, X. Li⁴⁸, Y. Li⁵⁷, Y. Liang²⁹, R. Licenik³⁸, T. Lin⁵⁵, Y. Lin¹¹, M. A. Lisa³⁹,
F. Liu¹¹, H. Liu²⁵, P. Liu⁵², P. Liu⁵⁰, T. Liu⁶⁴, X. Liu³⁹, Y. Liu⁵⁵, Z. Liu⁴⁸,
T. Ljubicic⁶, W. J. Llope⁶³, R. S. Longacre⁶, N. S. Lukow⁵⁴, S. Luo¹², X. Luo¹¹,
G. L. Ma⁵⁰, L. Ma¹⁸, R. Ma⁶, Y. G. Ma⁵⁰, N. Magdy¹², R. Majka⁶⁴, D. Mallick³⁶,
S. Margetis²⁹, C. Markert⁵⁶, H. S. Matis³¹, J. A. Mazer⁴⁶, N. G. Minaev⁴³,
S. Mioduszewski⁵⁵, B. Mohanty³⁶, M. M. Mondal⁵², I. Mooney⁶³, Z. Moravcova¹⁴,
D. A. Morozov⁴³, M. Nagy¹⁶, J. D. Nam⁵⁴, Md. Nasim²², K. Nayak¹¹, D. Neff⁹,
J. M. Nelson⁷, D. B. Nemes⁶⁴, M. Nie⁴⁹, G. Nigmatkulov³⁵, T. Niida⁵⁸,
L. V. Nogach⁴³, T. Nonaka⁵⁸, A. S. Nunes⁶, G. Odyniec³¹, A. Ogawa⁶, S. Oh³¹,
V. A. Okorokov³⁵, B. S. Page⁶, R. Pak⁶, A. Pandav³⁶, Y. Panebratsev²⁸, B. Pawlik⁴⁰,
D. Pawlowska⁶², H. Pei¹¹, C. Perkins⁷, L. Pinsky²⁰, R. L. Pintér¹⁶, J. Pluta⁶²,
J. Porter³¹, M. Posik⁵⁴, N. K. Pruthi⁴¹, M. Przybycien², J. Putschke⁶³, H. Qiu²⁶,
A. Quintero⁵⁴, S. K. Radhakrishnan²⁹, S. Ramachandran³⁰, R. L. Ray⁵⁶, R. Reed³²,
H. G. Ritter³¹, J. B. Roberts⁴⁵, O. V. Rogachevskiy²⁸, J. L. Romero⁸, L. Ruan⁶,

J. Rusnak³⁸, N. R. Sahoo⁴⁹, H. Sako⁵⁸, S. Salur⁴⁶, J. Sandweiss⁶⁴, S. Sato⁵⁸,
W. B. Schmidke⁶, N. Schmitz³³, B. R. Schweid⁵², F. Seck¹⁵, J. Seger¹³, M. Sergeeva⁹,
R. Seto¹⁰, P. Seyboth³³, N. Shah²⁴, E. Shahaliev²⁸, P. V. Shanmuganathan⁶,
M. Shao⁴⁸, F. Shen⁴⁹, W. Q. Shen⁵⁰, S. S. Shi¹¹, Q. Y. Shou⁵⁰, E. P. Sichtermann³¹,
R. Sikora², M. Simko³⁸, J. Singh⁴¹, S. Singha²⁶, N. Smirnov⁶⁴, W. Solyst²⁵,
P. Sorensen⁶, H. M. Spinka⁴, B. Srivastava⁴⁴, T. D. S. Stanislaus⁶⁰, M. Stefaniak⁶²,
D. J. Stewart⁶⁴, M. Strikhanov³⁵, B. Stringfellow⁴⁴, A. A. P. Suaide⁴⁷, M. Sumbera³⁸,
B. Summa⁴², X. M. Sun¹¹, X. Sun¹², Y. Sun⁴⁸, Y. Sun²¹, B. Surrow⁵⁴, D. N. Svirida³,
P. Szymanski⁶², A. H. Tang⁶, Z. Tang⁴⁸, A. Taranenko³⁵, T. Tarnowsky³⁴,
J. H. Thomas³¹, A. R. Timmins²⁰, D. Tlusty¹³, M. Tokarev²⁸, C. A. Tomkiel³²,
S. Trentalange⁹, R. E. Tribble⁵⁵, P. Tribedy⁶, S. K. Tripathy¹⁶, O. D. Tsai⁹, Z. Tu⁶,
T. Ullrich⁶, D. G. Underwood⁴, I. Upsal^{49,6}, G. Van Buren⁶, J. Vanek³⁸,
A. N. Vasiliev⁴³, I. Vassiliev¹⁷, F. Videbæk⁶, S. Vokal²⁸, S. A. Voloshin⁶³, F. Wang⁴⁴,
G. Wang⁹, J. S. Wang²¹, P. Wang⁴⁸, Y. Wang¹¹, Y. Wang⁵⁷, Z. Wang⁴⁹, J. C. Webb⁶,
P. C. Weidenkaff¹⁹, L. Wen⁹, G. D. Westfall³⁴, H. Wieman³¹, S. W. Wissink²⁵,
R. Witt⁵⁹, Y. Wu¹⁰, Z. G. Xiao⁵⁷, G. Xie³¹, W. Xie⁴⁴, H. Xu²¹, N. Xu³¹, Q. H. Xu⁴⁹,
Y. F. Xu⁵⁰, Y. Xu⁴⁹, Z. Xu⁶, Z. Xu⁹, C. Yang⁴⁹, Q. Yang⁴⁹, S. Yang⁶, Y. Yang³⁷,
Z. Yang¹¹, Z. Ye⁴⁵, Z. Ye¹², L. Yi⁴⁹, K. Yip⁶, H. Zbroszczyk⁶², W. Zha⁴⁸, C. Zhang⁵²,
D. Zhang¹¹, S. Zhang⁴⁸, S. Zhang⁵⁰, X. P. Zhang⁵⁷, Y. Zhang⁴⁸, Y. Zhang¹¹,
Z. J. Zhang³⁷, Z. Zhang⁶, Z. Zhang¹², J. Zhao⁴⁴, C. Zhong⁵⁰, C. Zhou⁵⁰, X. Zhu⁵⁷,
Z. Zhu⁴⁹, M. Zurek³¹, M. Zyzak¹⁷

(STAR Collaboration)

¹ Abilene Christian University, Abilene, Texas 79699

² AGH University of Science and Technology, FPACS, Cracow 30-059, Poland

³ Alikhanov Institute for Theoretical and Experimental Physics NRC "Kurchatov Institute", Moscow 117218, Russia

⁴ Argonne National Laboratory, Argonne, Illinois 60439

⁵ American University of Cairo, New Cairo 11835, New Cairo, Egypt

⁶ Brookhaven National Laboratory, Upton, New York 11973

⁷ University of California, Berkeley, California 94720

⁸ University of California, Davis, California 95616

⁹ University of California, Los Angeles, California 90095

¹⁰ University of California, Riverside, California 92521

¹¹ Central China Normal University, Wuhan, Hubei 430079

¹² University of Illinois at Chicago, Chicago, Illinois 60607

¹³ Creighton University, Omaha, Nebraska 68178

¹⁴ Czech Technical University in Prague, FNSPE, Prague 115 19, Czech Republic

¹⁵ Technische Universität Darmstadt, Darmstadt 64289, Germany

¹⁶ ELTE Eötvös Loránd University, Budapest, Hungary H-1117

¹⁷ Frankfurt Institute for Advanced Studies FIAS, Frankfurt 60438, Germany

¹⁸ Fudan University, Shanghai, 200433

- ¹⁹ *University of Heidelberg, Heidelberg 69120, Germany*
- ²⁰ *University of Houston, Houston, Texas 77204*
- ²¹ *Huzhou University, Huzhou, Zhejiang 313000*
- ²² *Indian Institute of Science Education and Research (IISER), Berhampur 760010, India*
- ²³ *Indian Institute of Science Education and Research (IISER) Tirupati, Tirupati 517507, India*
- ²⁴ *Indian Institute Technology, Patna, Bihar 801106, India*
- ²⁵ *Indiana University, Bloomington, Indiana 47408*
- ²⁶ *Institute of Modern Physics, Chinese Academy of Sciences, Lanzhou, Gansu 730000*
- ²⁷ *University of Jammu, Jammu 180001, India*
- ²⁸ *Joint Institute for Nuclear Research, Dubna 141 980, Russia*
- ²⁹ *Kent State University, Kent, Ohio 44242*
- ³⁰ *University of Kentucky, Lexington, Kentucky 40506-0055*
- ³¹ *Lawrence Berkeley National Laboratory, Berkeley, California 94720*
- ³² *Lehigh University, Bethlehem, Pennsylvania 18015*
- ³³ *Max-Planck-Institut für Physik, Munich 80805, Germany*
- ³⁴ *Michigan State University, East Lansing, Michigan 48824*
- ³⁵ *National Research Nuclear University MEPhI, Moscow 115409, Russia*
- ³⁶ *National Institute of Science Education and Research, HBNI, Jatni 752050, India*
- ³⁷ *National Cheng Kung University, Tainan 70101*
- ³⁸ *Nuclear Physics Institute of the CAS, Rez 250 68, Czech Republic*
- ³⁹ *Ohio State University, Columbus, Ohio 43210*
- ⁴⁰ *Institute of Nuclear Physics PAN, Cracow 31-342, Poland*
- ⁴¹ *Panjab University, Chandigarh 160014, India*
- ⁴² *Pennsylvania State University, University Park, Pennsylvania 16802*
- ⁴³ *NRC "Kurchatov Institute", Institute of High Energy Physics, Protvino 142281, Russia*
- ⁴⁴ *Purdue University, West Lafayette, Indiana 47907*
- ⁴⁵ *Rice University, Houston, Texas 77251*
- ⁴⁶ *Rutgers University, Piscataway, New Jersey 08854*
- ⁴⁷ *Universidade de São Paulo, São Paulo, Brazil 05314-970*
- ⁴⁸ *University of Science and Technology of China, Hefei, Anhui 230026*
- ⁴⁹ *Shandong University, Qingdao, Shandong 266237*
- ⁵⁰ *Shanghai Institute of Applied Physics, Chinese Academy of Sciences, Shanghai 201800*
- ⁵¹ *Southern Connecticut State University, New Haven, Connecticut 06515*
- ⁵² *State University of New York, Stony Brook, New York 11794*
- ⁵³ *Instituto de Alta Investigación, Universidad de Tarapacá, Chile*
- ⁵⁴ *Temple University, Philadelphia, Pennsylvania 19122*

⁵⁵ *Texas A&M University, College Station, Texas 77843*

⁵⁶ *University of Texas, Austin, Texas 78712*

⁵⁷ *Tsinghua University, Beijing 100084*

⁵⁸ *University of Tsukuba, Tsukuba, Ibaraki 305-8571, Japan*

⁵⁹ *United States Naval Academy, Annapolis, Maryland 21402*

⁶⁰ *Valparaiso University, Valparaiso, Indiana 46383*

⁶¹ *Variable Energy Cyclotron Centre, Kolkata 700064, India*

⁶² *Warsaw University of Technology, Warsaw 00-661, Poland*

⁶³ *Wayne State University, Detroit, Michigan 48201*

⁶⁴ *Yale University, New Haven, Connecticut 06520*

Abstract

Flow harmonics (v_n) of the Fourier expansion for the azimuthal distributions of hadrons are commonly employed to quantify the azimuthal anisotropy of particle production relative to the collision symmetry planes. While lower order Fourier coefficients (v_2 and v_3) are more directly related to the corresponding eccentricities of the initial state, the higher-order flow harmonics ($v_{n>3}$) can be induced by a mode-coupled response to the lower-order anisotropies, in addition to a linear response to the same-order anisotropies. These higher-order flow harmonics and their linear and mode-coupled contributions can be used to more precisely constrain the initial conditions and the transport properties of the medium in theoretical models. The multiparticle azimuthal cumulant method is used to measure the linear and mode-coupled contributions in the higher-order anisotropic flow, the mode-coupled response coefficients, and the correlations of the event plane angles for charged particles as functions of centrality and transverse momentum in Au+Au collisions at nucleon-nucleon center-of-mass energy $\sqrt{s_{NN}} = 200$ GeV. The results are compared to similar LHC measurements as well as to several viscous hydrodynamic calculations with varying initial conditions.

Keywords: Collectivity, correlation, shear viscosity

PACS: 25.75.-Ld

1. Introduction

Experimental studies of heavy-ion collisions at the Relativistic Heavy Ion Collider (RHIC) indicate that a state of matter predicted by Quantum Chromodynamics (QCD), called Quark-Gluon Plasma (QGP), is formed in these collisions. Many of the ongoing studies are aimed at characterizing the transport properties (particularly, the specific shear viscosity: the ratio of shear viscosity to entropy density η/s) of the QGP. The azimuthal anisotropy of particle production relative to the collision symmetry planes, known as anisotropic flow, is a key observable in many such studies because it displays

the viscous hydrodynamic response to the initial spatial distribution created in the early stages of the collision [1–14].

The anisotropic flow can be characterized by the Fourier expansion [15] of the particle azimuthal angle (ϕ) distributions,

$$\frac{dN}{d\phi} = \frac{N}{2\pi} \left(1 + 2 \sum_{n=1} V_n e^{-in\phi} \right), \quad (1)$$

where $V_n = v_n e^{in\Psi_n}$ is the n -th complex anisotropic flow vector, v_n and Ψ_n represent the vector magnitude and direction, respectively. The flow coefficient v_1 is commonly termed as directed flow, v_2 is the elliptic flow, and v_3 is the triangular flow. Anisotropic flow studies of higher-order flow harmonics $v_{n>3}$ [10, 16–22], correlation between different flow harmonics [20, 23–27] and flow fluctuations [18, 28–30] have led to a deeper understanding of the initial conditions [31] and the properties of the matter created in heavy-ion collisions.

In the hydrodynamic models, anisotropic flow arises from the evolution of the medium in the presence of initial-state energy density anisotropies, characterized by the complex eccentricity vectors [24, 32–35]:

$$\mathcal{E}_n \equiv \varepsilon_n e^{in\Phi_n} \equiv - \frac{\int d^2r_{\perp} r^n e^{in\varphi} \rho_e(r, \varphi)}{\int d^2r_{\perp} r^n \rho_e(r, \varphi)}, \quad (n > 1), \quad (2)$$

where $\rho_e(r, \varphi)$ is the initial anisotropic density profile, $\varepsilon_n = \langle |\mathcal{E}_n|^2 \rangle^{1/2}$ represents the eccentricity vectors magnitude and Φ_n denotes the azimuthal direction of the eccentricity vector [35–37].

The elliptic and triangular flow harmonics are, to a reasonable approximation, linearly proportional to the initial-state anisotropies, ε_2 and ε_3 , respectively [7, 24, 38–44]:

$$v_n = k_n \varepsilon_n, \quad (3)$$

where k_n is the proportionality factor that encodes the medium response, and is expected to be sensitive to η/s and the system lifetime [45]. Therefore, the ratio v_n / ε_n (for $n = 2, 3$) could be used as a tool to probe η/s of the QGP [17]. In contrast, the higher-order flow harmonics are expected to arise from a mode-coupled (nonlinear) response to the lower-order eccentricities, ε_2 and/or ε_3 [12, 36, 37] in addition to linear response to the same-order initial-state anisotropies [46]:

$$V_4 = V_4^L + V_4^{\text{mc}} = V_4^L + \chi_{4,22} V_2 V_2, \quad (4)$$

$$V_5 = V_5^L + V_5^{\text{mc}} = V_5^L + \chi_{5,23} V_2 V_3, \quad (5)$$

where V_n^L and V_n^{mc} represents the linear and the mode-coupled contributions to the flow vector V_n respectively. The $\chi_{4,22}$ and $\chi_{5,23}$ are the mode-coupled response coefficients which define the magnitude of the $V_{n>3}^{\text{mc}}$ measured with respect to the lower-order symmetry plane angle(s). Also, the mode-coupled contribution of V_n is expected to reflect the correlation between different order flow symmetry planes, Ψ_n , which could shed light on the initial stage dynamics [23, 27, 36, 47–53].

The v_2 and v_3 harmonics are sensitive to the respective influence of the initial-state eccentricity and the final-state viscous attenuation, which have proven difficult to disentangle. The mode-coupled coefficients show characteristically different dependencies on the viscous attenuation and the initial-state eccentricity [44]. Therefore, they can be used in conjunction with measurements for the v_2 and v_3 harmonics to leverage additional unique constraints for initial-state models, as well as reliable extraction of transport coefficients.

In this paper we report new differential and integral measurements of v_4 and v_5 and their mode-coupled response coefficients, obtained with the two- and multiparticle cumulant methods described in Section 2. Measurements of these quantities as functions of collision centrality and charged particle transverse momentum, p_T , in Au+Au collisions at $\sqrt{s_{NN}} = 200$ GeV, are reported in Section 3. The presented results and conclusions are summarized in Section 4.

2. Experimental setup and analysis method

2.1. Experimental setup

The data reported in this analysis were collected with the STAR detector at RHIC using a minimum-bias trigger [54] in 2011. Charged particle tracks, measured in pseudorapidity range $|\eta| < 1.0$ and covering all azimuthal angles of the Time Projection Chamber (TPC) [55], are used to reconstruct the collision vertices. Collision centrality is determined from the measured event-by-event multiplicity with the assistance of the Monte Carlo Glauber simulation [56]. Tracks included in the analysis are required to have a distance of closest approach to the primary vertex of less than 3 cm, and to have at least 15 TPC space points used in their reconstruction. In order to remove track splitting, the ratio of the number of fit points to the maximum possible number of TPC fit points was required to be larger than 0.52. Tracks used in this study are restricted to transverse momentum $0.2 < p_T < 4$ GeV/ c . Events are chosen with vertex positions within ± 30 cm from the TPC center (along the beam direction), and within ± 2 cm in the radial direction relative to the center of the beam intersection. Also, the absolute difference between the two z -vertex positions defined by the TPC and Vertex Position Detector is required to be less than 3 cm to decrease beam-induced background and pileup.

The systematic uncertainties associated with the measurements presented in this work are estimated by changing different parameters of the analysis and comparing the results with their baseline values. The systematic uncertainty associated with the event selection is estimated by using more restrictive requirements for the vertex positions determined by the TPC along the beam direction (-30 to 0 cm or 0 to 30 cm instead of the nominal value of ± 30 cm). The systematic uncertainty arising from track selection is evaluated by employing more strict requirements: (i) Distance of Closest Approach (DCA) is changed to be less than 2 cm instead of the standard value of 3 cm, and (ii) number of TPC space points from more than 15 points to more than 20 points. The systematic uncertainty associated with the nonflow effects, due to Bose-Einstein correlations, resonance decays and the fragments of individual jets, is estimated by investigating the impact of a pseudorapidity gap, $\Delta\eta = \eta_1 - \eta_2$, for the track pairs used in the measurements. Studies were performed for $\Delta\eta$ values of 0.6, 0.7, and 1.0.

Table 1 shows the systematic uncertainties evaluated for this work. The overall systematic uncertainty was calculated by combining uncertainties from different sources in quadrature. In the ensuing figures, the overall systematic uncertainties (which do not include those from $\Delta\eta$ variation) are shown as open boxes; statistical uncertainties are shown as vertical lines.

Variations of Quantities	Minimum value	Maximum value
Event	2%	4%
Track	3%	6%
$\Delta\eta$	3%	8%

Table 1: The contributions to the total systematic uncertainties from various sources.

2.2. Analysis method

The two- and multiparticle cumulant techniques are used in this work. The framework for the cumulant method is described in Refs. [47, 57], which was extended to the case of subevents in Refs. [58, 59]. In this work, the two- and multiparticle correlations were constructed using the two-subevents cumulant method [59], with particle weights, e.g. weighted with the particles acceptance correction, and $\Delta\eta > 0.7$ separation between the subevents A and B (*i.e.*, $\eta_A > 0.35$ and $\eta_B < -0.35$). The use of the two-subevents method helps to suppress the nonflow correlations. The two- and multiparticle correlations are written as:

$$v_k^{\text{Inclusive}} = \langle\langle \cos(k(\varphi_1^A - \varphi_2^B)) \rangle\rangle^{1/2}, \quad (6)$$

$$C_{k,nm} = \langle\langle \cos(k\varphi_1^A - n\varphi_2^B - m\varphi_3^B) \rangle\rangle, \quad (7)$$

$$\langle v_n^2 v_m^2 \rangle = \langle\langle \cos(n\varphi_1^A + m\varphi_2^A - n\varphi_3^B - m\varphi_4^B) \rangle\rangle, \quad (8)$$

where $\langle\langle \rangle\rangle$ indicates the average over all particles in a single event and then the average over all events, $k = n + m$, $n = 2$, $m = 2$ or 3 , and φ_i is the azimuthal angle of the i -th particle.

Using Eqs. (6)-(8), the mode-coupled contribution in higher-order anisotropic flow harmonics, v_4 and v_5 , can be expressed as [37, 60]:

$$v_4^{\text{mc}} = \frac{C_{4,22}}{\sqrt{\langle v_2^2 v_2^2 \rangle}}, \quad (9)$$

$$\sim \langle v_4 \cos(4\Psi_4 - 2\Psi_2 - 2\Psi_2) \rangle,$$

$$v_5^{\text{mc}} = \frac{C_{5,23}}{\sqrt{\langle v_2^2 v_3^2 \rangle}}, \quad (10)$$

$$\sim \langle v_5 \cos(5\Psi_5 - 2\Psi_2 - 3\Psi_3) \rangle,$$

and the linear contribution to v_4 and v_5 can be given as:

$$v_4^L = \sqrt{(v_4^{\text{Inclusive}})^2 - (v_4^{\text{mc}})^2}, \quad (11)$$

$$v_5^L = \sqrt{(v_5^{\text{Inclusive}})^2 - (v_5^{\text{mc}})^2}.$$

Equation (11) assumes that the linear and mode-coupled contributions in v_4 and v_5 are independent [37, 61]. The ratios of the mode-coupled contribution to the inclusive v_4 and v_5 are expected to measure the correlations between different order flow symmetry planes [62] and are expressed as $\rho_{4,22}$ and $\rho_{5,23}$, respectively. The $\rho_{4,22}$ and $\rho_{5,23}$ can be given as:

$$\rho_{4,22} = \frac{v_4^{\text{mc}}}{v_4^{\text{Inclusive}}} = \langle \cos(4\Psi_4 - 2\Psi_2 - 2\Psi_2) \rangle, \quad (12)$$

$$\rho_{5,23} = \frac{v_5^{\text{mc}}}{v_5^{\text{Inclusive}}} = \langle \cos(5\Psi_5 - 2\Psi_2 - 3\Psi_3) \rangle. \quad (13)$$

The mode-coupled response coefficients, $\chi_{4,22}$ and $\chi_{5,23}$, which quantify the contributions of the mode-coupling to the the higher-order anisotropic flow harmonics, are defined as

$$\chi_{4,22} = \frac{v_4^{\text{mc}}}{\sqrt{\langle v_2^2 v_2^2 \rangle}} \quad (14)$$

$$\chi_{5,23} = \frac{v_5^{\text{mc}}}{\sqrt{\langle v_2^2 v_3^2 \rangle}}. \quad (15)$$

In Eq.(15) for the differential $\chi_{5,23}$, this work further makes the approximation $\langle v_2^2 v_3^2 \rangle \sim \langle v_2^2 \rangle \langle v_3^2 \rangle$ [36]. These dimensionless ratios that represent the mode-coupled coefficients in Eq.(4) are expected to be weakly sensitive to viscous effects [44].

3. Results and discussion

In A+A collisions, short-range nonflow correlations contribute to the measured three-particle correlators $C_{4,22}$ and $C_{5,23}$ [61]. However, such correlations can be reduced by using subevents cumulant methods [59]. Figure 1 compares the $C_{4,22}$ and $C_{5,23}$ values obtained from the standard (*i.e.*, the three particles are selected using the entire detector acceptance) and the two-subevents cumulant methods as a function of centrality in the range $0.2 < p_T < 4.0$ GeV/ c for Au+Au collisions at $\sqrt{s_{NN}}=200$ GeV. The magnitudes of the measured $C_{4,22}$ and $C_{5,23}$ from the standard cumulant method are larger than those from the subevents cumulant method, compatible with the expectation that the subevents cumulant method can further reduce the nonflow correlations. The shaded bands in Fig. 1 indicate viscous hydrodynamic model predictions [63, 64], as summarized in Table 2. Note that these model predictions include an influence from changes in the initial- and final-state assumptions incorporated in model calculations. The model predictions, which were generated with the standard cumulant method, show good qualitative agreement with both $C_{4,22}$ and $C_{5,23}$. However, Hydro-2^b with no hadronic cascade gives a better description of the data for $C_{4,22}$ and $C_{5,23}$ obtained with the two-subevents cumulant method.

The centrality dependence of the inclusive, linear and mode-coupled v_4 and v_5 in the p_T range from 0.2 to 4.0 GeV/ c for Au+Au collisions at $\sqrt{s_{NN}}=200$ GeV are shown in Fig. 2. They indicate that the linear mode of v_4 and v_5 depends weakly on the collision centrality and constitutes the dominant contribution to the inclusive v_4 and v_5 in central collisions. These results are compared to similar LHC measurements in the p_T range from

	Hydro-1 [63]	Hydro-2 ^{a/b} [64]
η/s	0.05	0.12
Initial conditions	TRENTO Initial conditions	IP-Glasma Initial conditions
Contributions	Hydro + Direct decays	(a) Hydro + Hadronic cascade (b) Hydro only

Table 2: Summary description of the hydrodynamic simulations, Hydro-1 [63], and Hydro-2^{a/b} [64].

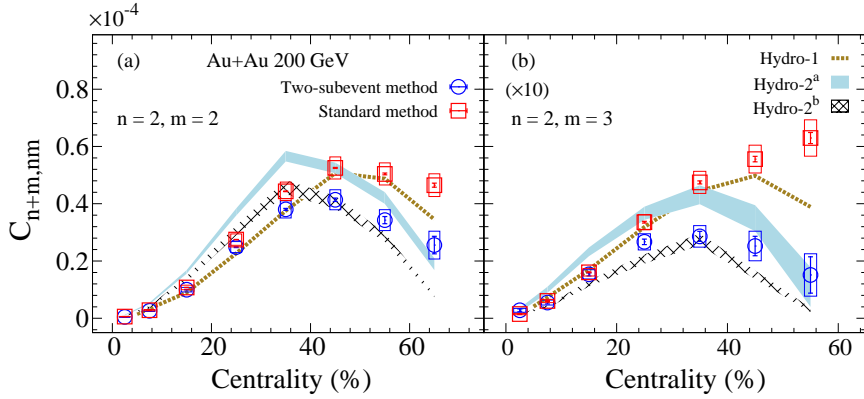


Figure 1: Comparison of the p_T -integrated three-particle correlators, $C_{4,22}$ and $C_{5,23}$, for Au+Au collisions at $\sqrt{s_{NN}}=200$ GeV, obtained with the standard (red squares) and the two-subevents cumulant (blue circles) methods. The respective systematic uncertainties, that do not include the nonflow contributions, are shown as open boxes. The vertical lines represent the statistical errors. The shaded bands indicate hydrodynamic model predictions Hydro-1 [63], Hydro-2^a and Hydro-2^b [64].

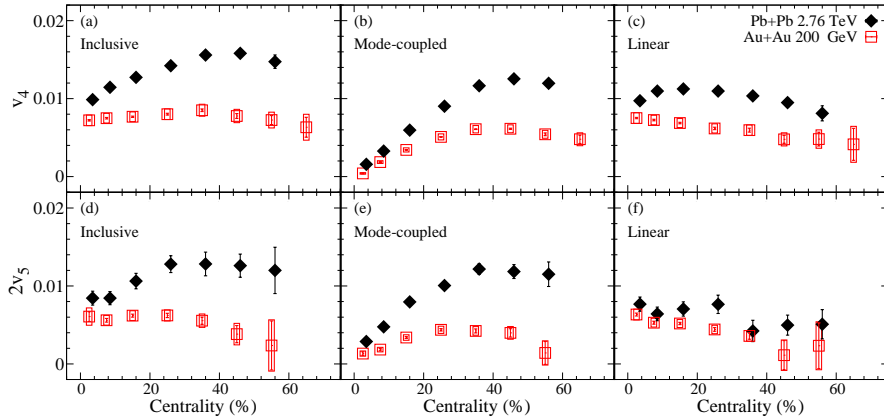


Figure 2: Comparison of the inclusive mode-coupled and linear higher-order flow harmonics v_4 and v_5 obtained with the two-subevents cumulant method, as a function of centrality in the p_T range 0.2 – 4.0 GeV/ c for Au+Au collisions at $\sqrt{s_{NN}}=200$ GeV. The systematic uncertainties, that do not include the nonflow contributions, are shown as open boxes. The solid diamonds indicate LHC measurements for the p_T range from 0.2 – 5.0 GeV/ c for Pb+Pb collisions at $\sqrt{s_{NN}}=2.76$ TeV [62].

0.2 to 5.0 GeV/ c and pseudorapidity range $|\eta| < 0.8$ for Pb+Pb collisions at $\sqrt{s_{NN}}=2.76$ TeV [62]. The comparison indicates strikingly similar patterns for the RHIC and

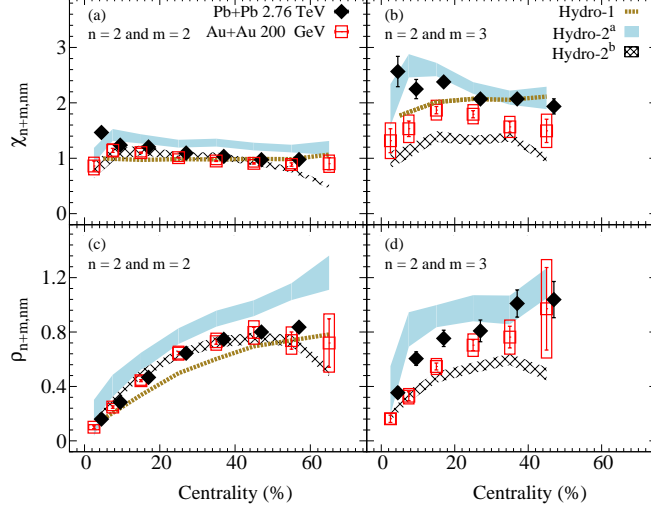


Figure 3: Results as a function of centrality in the p_T range from 0.2 to 4.0 GeV/c for Au+Au collisions at $\sqrt{s_{NN}} = 200$ GeV. Panels (a) and (b) show the mode-coupled response coefficients, $\chi_{4,22}$ and $\chi_{5,23}$, and panels (c) and (d) show the correlations of event plane angles, $\rho_{4,22}$ and $\rho_{5,23}$. The results were obtained with the two-subevents cumulant method; the open boxes indicate the systematic uncertainties. The closed-symbols represent similar LHC measurements in the p_T range from 0.2 to 5.0 GeV/c for Pb+Pb collisions at $\sqrt{s_{NN}} = 2.76$ TeV [62]. The shaded bands indicate hydrodynamic model predictions Hydro-1 [63], Hydro-2^a and Hydro-2^b [64].

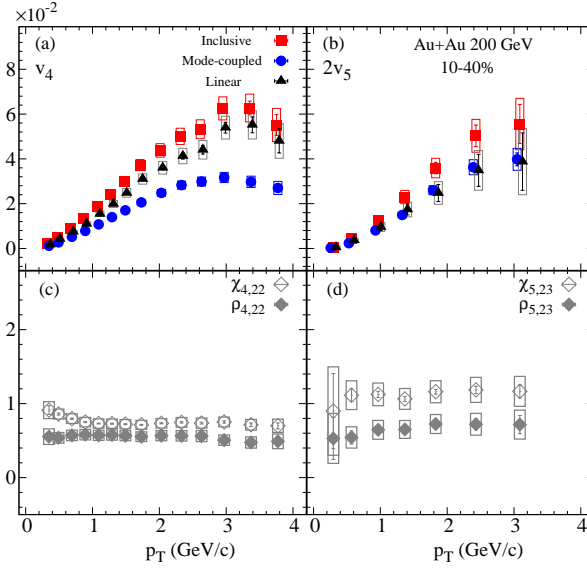


Figure 4: Results as a function of p_T for 10-40% central Au+Au collisions at $\sqrt{s_{NN}} = 200$ GeV. Panels (a) and (b) present the inclusive, linear and mode-coupled higher-order flow harmonics v_4 and v_5 obtained with the two-subevents cumulant method. Panel (c) presents the $\chi_{4,22}$ and $\rho_{4,22}$, while panel (d) presents the $\chi_{5,23}$ and $\rho_{5,23}$. The open boxes indicate the systematic uncertainties.

LHC measurements, albeit with a difference in the magnitude of the measurements. This

observed difference could result from a sizable difference in the $\langle p_T \rangle$ for the p_T -integrated v_4 and v_5 measurements at RHIC and the LHC, respectively. Here, it is noteworthy that even though the p_T range for both measurements is similar, the inverse slopes of the hadron p_T spectra are larger at the LHC than at RHIC. Subtleties related to a difference in the viscous properties of the medium created at RHIC and LHC energies could also contribute to the observed difference in the magnitude of the measurements [63].

The centrality dependence of the mode-coupled response coefficients, $\chi_{4,22}$ and $\chi_{5,23}$, for Au+Au collisions, is presented in Fig. 3(a) and (b) for the range $0.2 < p_T < 4.0$ GeV/ c . They show a weak centrality dependence, akin to the patterns observed for similar measurements at the LHC for Pb+Pb collisions at $\sqrt{s_{NN}} = 2.76$ TeV [62] (closed symbols). These patterns suggest that (i) the centrality dependence observed for the mode-coupled v_4 and v_5 (*cf.*, Figs. 2(b) and (e)) stems from the lower-order flow harmonics and (ii) the mode-coupled response coefficients are dominated by initial-state eccentricity couplings which have a weak dependence on beam energy. The shaded bands in Figs. 3(a) and (b) show that the predictions from the viscous hydrodynamic models [63, 64] summarized in Table 2, give a good qualitative description of the $\chi_{4,22}$ and $\chi_{5,23}$ data. However, the predictions from Hydro-1 and Hydro-2^b (*cf.* Table 2), give the overall closest description to $\chi_{4,22}$ and $\chi_{5,23}$.

Figures 3(c) and (d) show the centrality dependence of the correlations of the event plane angles, $\rho_{4,22}$ and $\rho_{5,23}$, for $0.2 < p_T < 4.0$ GeV/ c in Au+Au collisions at $\sqrt{s_{NN}} = 200$ GeV. The data suggest stronger event plane correlations in peripheral than in central collisions. This centrality dependent pattern is also captured by the viscous hydrodynamic model predictions [63, 64] indicated by the shaded bands in the figure. The LHC $\rho_{4,22}$ and $\rho_{5,23}$ measurements for Pb+Pb collisions at $\sqrt{s_{NN}} = 2.76$ TeV [62] (closed symbols), also indicate magnitudes and trends similar to those for the Au+Au collisions. This observation could be an indication that the correlation of event plane angles are dominated by initial-state effects.

The p_T dependence of the inclusive, linear and mode-coupled higher-order flow harmonics, v_4 and v_5 , for 10-40% central Au+Au collisions, are compared in Figs. 4(a) and (b). They show that the p_T -dependent trends of the linear and mode-coupled contributions are similar to the inclusive v_4 and v_5 , as previously measured by the STAR collaboration [10, 19]. This observation suggests that the linear and mode-coupled contributions are driven by the same p_T -dependent physics processes. The corresponding mode-coupled response coefficients $\chi_{4,22}$ and $\chi_{5,23}$ and the correlations of event plane angles $\rho_{4,22}$ and $\rho_{5,23}$ are shown in Figs. 4 (c) and (d). They indicate little, if any, p_T dependence for the centrality selection presented. These trends suggest that both dimensionless coefficients are dominated by initial-state effects.

4. Summary

In summary, we have presented new differential measurements of the charge-inclusive, linear and mode-coupled contributions to the higher-order anisotropic flow coefficients v_4 and v_5 , mode-coupled response coefficients $\chi_{4,22}$ and $\chi_{5,23}$ and the correlations of the event plane angles $\rho_{4,22}$ and $\rho_{5,23}$, for Au+Au collisions at $\sqrt{s_{NN}} = 200$ GeV. The p_T -integrated measurements indicate a sizable centrality dependence for the mode-coupled contributions of v_4 and v_5 , whereas the linear contributions, that dominate the central collisions, show a weak centrality dependence. The v_4 and v_5 results are compared with

similar LHC measurements which show larger magnitude that could be driven by the difference in the viscous effects and the mean p_T between RHIC and LHC energies. The $\chi_{4,22}$ and $\chi_{5,23}$ show a weak centrality dependence, however the $\rho_{4,22}$ and $\rho_{5,23}$ increase from central to peripheral collisions. These dimensionless coefficients show magnitudes and trends which are similar to those observed for LHC measurements, suggesting that the correlations of event plane angles as well as the mode-coupled response coefficients are dominated by initial-state effects. This is further supported by the observed p_T independence of the $\chi_{4,22}$, $\chi_{5,23}$, $\rho_{4,22}$ and $\rho_{5,23}$. Viscous hydrodynamic model comparisons to the data indicate good qualitative agreement. However, none of the models provide a simultaneous description of the three-particle correlations, the mode-coupled response coefficients, and the correlations of event plane angles. These higher-order flow measurements could provide additional stringent constraints to discern between initial state models and aid precision extraction of the transport properties of the medium produced in the collisions.

Acknowledgments

We thank the RHIC Operations Group and RCF at BNL, the NERSC Center at LBNL, and the Open Science Grid consortium for providing resources and support. This work was supported in part by the Office of Nuclear Physics within the U.S. DOE Office of Science, the U.S. National Science Foundation, the Ministry of Education and Science of the Russian Federation, National Natural Science Foundation of China, Chinese Academy of Science, the Ministry of Science and Technology of China and the Chinese Ministry of Education, the Higher Education Sprout Project by Ministry of Education at NCKU, the National Research Foundation of Korea, Czech Science Foundation and Ministry of Education, Youth and Sports of the Czech Republic, Hungarian National Research, Development and Innovation Office, New National Excellency Programme of the Hungarian Ministry of Human Capacities, Department of Atomic Energy and Department of Science and Technology of the Government of India, the National Science Centre of Poland, the Ministry of Science, Education and Sports of the Republic of Croatia, RosAtom of Russia and German Bundesministerium für Bildung, Wissenschaft, Forschung und Technologie (BMBF), Helmholtz Association, Ministry of Education, Culture, Sports, Science, and Technology (MEXT) and Japan Society for the Promotion of Science (JSPS).

References

References

- [1] U. Heinz, P. Kolb, Early thermalization at RHIC, Nucl. Phys. A702 (2002) 269–280.
- [2] T. Hirano, U. W. Heinz, D. Kharzeev, R. Lacey, Y. Nara, Hadronic dissipative effects on elliptic flow in ultrarelativistic heavy-ion collisions, Phys.Lett. B636 (2006) 299–304. [arXiv:nucl-th/0511046](#), [doi:10.1016/j.physletb.2006.03.060](#).
- [3] P. Huovinen, P. F. Kolb, U. W. Heinz, P. V. Ruuskanen, S. A. Voloshin, Radial and elliptic flow at RHIC: Further predictions, Phys. Lett. B503 (2001) 58–64.
- [4] T. Hirano, K. Tsuda, Collective flow and two pion correlations from a relativistic hydrodynamic model with early chemical freeze out, Phys. Rev. C66 (2002) 054905. [arXiv:nucl-th/0205043](#), [doi:10.1103/PhysRevC.66.054905](#).

- [5] P. Romatschke, U. Romatschke, Viscosity Information from Relativistic Nuclear Collisions: How Perfect is the Fluid Observed at RHIC?, *Phys.Rev.Lett.* 99 (2007) 172301. [arXiv:0706.1522](#), [doi:10.1103/PhysRevLett.99.172301](#).
- [6] M. Luzum, Flow fluctuations and long-range correlations: elliptic flow and beyond, *J. Phys. G38* (2011) 124026. [arXiv:1107.0592](#), [doi:10.1088/0954-3899/38/12/124026](#).
- [7] H. Song, S. A. Bass, U. Heinz, T. Hirano, C. Shen, 200 A GeV Au+Au collisions serve a nearly perfect quark-gluon liquid, *Phys. Rev. Lett.* 106 (2011) 192301, [Erratum: *Phys. Rev. Lett.*109,139904(2012)]. [arXiv:1011.2783](#), [doi:10.1103/PhysRevLett.106.192301](#), [doi:10.1103/PhysRevLett.109.139904](#).
- [8] J. Qian, U. W. Heinz, J. Liu, Mode-coupling effects in anisotropic flow in heavy-ion collisions, *Phys. Rev. C93* (2016) 064901. [arXiv:1602.02813](#), [doi:10.1103/PhysRevC.93.064901](#).
- [9] N. Magdy, Beam energy dependence of the anisotropic flow coefficients v_n , *PoS CPOD2017* (2018) 005.
- [10] N. Magdy, Viscous Damping of Anisotropic Flow in 7.7 to 200 GeV Au+Au Collisions, *J. Phys. Conf. Ser.* 779 (2017) 012060. [doi:10.1088/1742-6596/779/1/012060](#).
- [11] B. Schenke, S. Jeon, C. Gale, Anisotropic flow in $\sqrt{s} = 2.76$ TeV Pb+Pb collisions at the LHC, *Phys.Lett. B702* (2011) 59–63. [arXiv:1102.0575](#), [doi:10.1016/j.physletb.2011.06.065](#).
- [12] D. Teaney, L. Yan, Nonlinearities in the harmonic spectrum of heavy ion collisions with ideal and viscous hydrodynamics, *Phys. Rev. C86* (2012) 044908. [arXiv:1206.1905](#), [doi:10.1103/PhysRevC.86.044908](#).
- [13] F. G. Gardim, F. Grassi, M. Luzum, J.-Y. Ollitrault, Anisotropic flow in event-by-event ideal hydrodynamic simulations of $\sqrt{s_{NN}} = 200$ GeV Au+Au collisions, *Phys.Rev.Lett.* 109 (2012) 202302. [arXiv:1203.2882](#), [doi:10.1103/PhysRevLett.109.202302](#).
- [14] R. A. Lacey, D. Reynolds, A. Taranenko, N. N. Ajitanand, J. M. Alexander, F.-H. Liu, Y. Gu, A. Mwai, Acoustic scaling of anisotropic flow in shape-engineered events: implications for extraction of the specific shear viscosity of the quark gluon plasma, *J. Phys. G43* (2016) 10LT01. [arXiv:1311.1728](#), [doi:10.1088/0954-3899/43/10/10LT01](#).
- [15] A. M. Poskanzer, S. A. Voloshin, Methods for analyzing anisotropic flow in relativistic nuclear collisions, *Phys. Rev. C58* (1998) 1671–1678. [arXiv:nucl-ex/9805001](#), [doi:10.1103/PhysRevC.58.1671](#).
- [16] N. Magdy, Beam-energy dependence of the azimuthal anisotropic flow from RHIC. [arXiv:1909.09640](#).
- [17] J. Adam, et al., Azimuthal Harmonics in Small and Large Collision Systems at RHIC Top Energies, *Phys. Rev. Lett.* 122 (2019) 172301. [arXiv:1901.08155](#), [doi:10.1103/PhysRevLett.122.172301](#).
- [18] N. Magdy, Collision system and beam energy dependence of anisotropic flow fluctuations, *Nucl. Phys. A982* (2019) 255–258. [arXiv:1807.07638](#), [doi:10.1016/j.nuclphysa.2018.09.027](#).
- [19] L. Adamczyk, et al., Azimuthal anisotropy in Cu+Au collisions at $\sqrt{s_{NN}} = 200$ GeV, *Phys. Rev. C98* (2018) 014915. [arXiv:1712.01332](#), [doi:10.1103/PhysRevC.98.014915](#).
- [20] L. Adamczyk, et al., Harmonic decomposition of three-particle azimuthal correlations at energies available at the BNL Relativistic Heavy Ion Collider, *Phys. Rev. C98* (2018) 034918. [arXiv:1701.06496](#), [doi:10.1103/PhysRevC.98.034918](#).
- [21] B. Alver, G. Roland, Collision geometry fluctuations and triangular flow in heavy-ion collisions, *Phys. Rev. C81* (2010) 054905, [Erratum: *Phys. Rev.C82,039903(2010)*]. [arXiv:1003.0194](#), [doi:10.1103/PhysRevC.82.039903](#), [doi:10.1103/PhysRevC.81.054905](#).
- [22] S. Chatrchyan, et al., Measurement of higher-order harmonic azimuthal anisotropy in PbPb collisions at $\sqrt{s_{NN}} = 2.76$ TeV, *Phys. Rev. C89* (2014) 044906. [arXiv:1310.8651](#), [doi:10.1103/PhysRevC.89.044906](#).
- [23] J. Adam, et al., Correlation Measurements Between Flow Harmonics in Au+Au Collisions at RHIC, *Phys. Lett. B783* (2018) 459–465. [arXiv:1803.03876](#), [doi:10.1016/j.physletb.2018.05.076](#).
- [24] Z. Qiu, U. W. Heinz, Event-by-event shape and flow fluctuations of relativistic heavy-ion collision fireballs, *Phys. Rev. C84* (2011) 024911. [arXiv:1104.0650](#), [doi:10.1103/PhysRevC.84.024911](#).
- [25] A. Adare, et al., Measurements of Higher-Order Flow Harmonics in Au+Au Collisions at $\sqrt{s_{NN}} = 200$ GeV, *Phys. Rev. Lett.* 107 (2011) 252301. [arXiv:1105.3928](#), [doi:10.1103/PhysRevLett.107.252301](#).
- [26] G. Aad, et al., Measurement of event-plane correlations in $\sqrt{s_{NN}} = 2.76$ TeV lead-lead collisions with the ATLAS detector, *Phys. Rev. C90* (2014) 024905. [arXiv:1403.0489](#), [doi:10.1103/PhysRevC.90.024905](#).
- [27] G. Aad, et al., Measurement of the correlation between flow harmonics of different order in lead-lead collisions at $\sqrt{s_{NN}}=2.76$ TeV with the ATLAS detector, *Phys. Rev. C92* (2015) 034903. [arXiv:1504.01289](#), [doi:10.1103/PhysRevC.92.034903](#).

- [28] B. Alver, et al., Importance of correlations and fluctuations on the initial source eccentricity in high-energy nucleus-nucleus collisions, *Phys. Rev. C* 77 (2008) 014906. [arXiv:0711.3724](#), [doi:10.1103/PhysRevC.77.014906](#).
- [29] B. Alver, et al., Non-flow correlations and elliptic flow fluctuations in gold-gold collisions at $\sqrt{s_{NN}} = 200$ GeV, *Phys. Rev. C* 81 (2010) 034915. [arXiv:1002.0534](#), [doi:10.1103/PhysRevC.81.034915](#).
- [30] J.-Y. Ollitrault, A. M. Poskanzer, S. A. Voloshin, Effect of flow fluctuations and nonflow on elliptic flow methods, *Phys. Rev. C* 80 (2009) 014904. [arXiv:0904.2315](#), [doi:10.1103/PhysRevC.80.014904](#).
- [31] W. Busza, K. Rajagopal, W. van der Schee, Heavy Ion Collisions: The Big Picture, and the Big Questions, *Ann. Rev. Nucl. Part. Sci.* 68 (2018) 339–376. [arXiv:1802.04801](#), [doi:10.1146/annurev-nucl-101917-020852](#).
- [32] B. H. Alver, C. Gombeaud, M. Luzum, J.-Y. Ollitrault, Triangular flow in hydrodynamics and transport theory, *Phys. Rev. C* 82 (2010) 034913. [arXiv:1007.5469](#), [doi:10.1103/PhysRevC.82.034913](#).
- [33] H. Petersen, G.-Y. Qin, S. A. Bass, B. Muller, Triangular flow in event-by-event ideal hydrodynamics in Au+Au collisions at $\sqrt{s_{NN}} = 200A$ GeV, *Phys. Rev. C* 82 (2010) 041901. [arXiv:1008.0625](#), [doi:10.1103/PhysRevC.82.041901](#).
- [34] R. A. Lacey, R. Wei, J. Jia, N. N. Ajitanand, J. M. Alexander, A. Taranenko, Initial eccentricity fluctuations and their relation to higher-order flow harmonics, *Phys. Rev. C* 83 (2011) 044902. [arXiv:1009.5230](#), [doi:10.1103/PhysRevC.83.044902](#).
- [35] D. Teaney, L. Yan, Triangularity and Dipole Asymmetry in Heavy Ion Collisions, *Phys. Rev. C* 83 (2011) 064904. [arXiv:1010.1876](#), [doi:10.1103/PhysRevC.83.064904](#).
- [36] R. S. Bhalerao, J.-Y. Ollitrault, S. Pal, Characterizing flow fluctuations with moments, *Phys. Lett. B* 742 (2015) 94–98. [arXiv:1411.5160](#), [doi:10.1016/j.physletb.2015.01.019](#).
- [37] L. Yan, J.-Y. Ollitrault, $\nu_4, \nu_5, \nu_6, \nu_7$: Nonlinear hydrodynamic response versus LHC data, *Phys. Lett. B* 744 (2015) 82–87. [arXiv:1502.02502](#), [doi:10.1016/j.physletb.2015.03.040](#).
- [38] H. Niemi, G. S. Denicol, H. Holopainen, P. Huovinen, Event-by-event distributions of azimuthal asymmetries in ultrarelativistic heavy-ion collisions, *Phys. Rev. C* 87 (2013) 054901. [arXiv:1212.1008](#), [doi:10.1103/PhysRevC.87.054901](#).
- [39] F. G. Gardim, J. Noronha-Hostler, M. Luzum, F. Grassi, Effects of viscosity on the mapping of initial to final state in heavy ion collisions, *Phys. Rev. C* 91 (2015) 034902. [arXiv:1411.2574](#), [doi:10.1103/PhysRevC.91.034902](#).
- [40] J. Fu, Centrality dependence of mapping the hydrodynamic response to the initial geometry in heavy-ion collisions, *Phys. Rev. C* 92 (2015) 024904. [doi:10.1103/PhysRevC.92.024904](#).
- [41] H. Holopainen, H. Niemi, K. J. Eskola, Event-by-event hydrodynamics and elliptic flow from fluctuating initial states, *Phys. Rev. C* 83 (2011) 034901. [arXiv:1007.0368](#), [doi:10.1103/PhysRevC.83.034901](#).
- [42] G.-Y. Qin, H. Petersen, S. A. Bass, B. Muller, Translation of collision geometry fluctuations into momentum anisotropies in relativistic heavy-ion collisions, *Phys. Rev. C* 82 (2010) 064903. [arXiv:1009.1847](#), [doi:10.1103/PhysRevC.82.064903](#).
- [43] C. Gale, S. Jeon, B. Schenke, P. Tribedy, R. Venugopalan, Event-by-event anisotropic flow in heavy-ion collisions from combined Yang-Mills and viscous fluid dynamics, *Phys. Rev. Lett.* 110 (2013) 012302. [arXiv:1209.6330](#), [doi:10.1103/PhysRevLett.110.012302](#).
- [44] P. Liu, R. A. Lacey, Acoustic scaling of linear and mode-coupled anisotropic flow; implications for precision extraction of the specific shear viscosity, *Phys. Rev. C* 98 (2018) 021902. [arXiv:1802.06595](#), [doi:10.1103/PhysRevC.98.021902](#).
- [45] U. Heinz, R. Snellings, Collective flow and viscosity in relativistic heavy-ion collisions, *Ann. Rev. Nucl. Part. Sci.* 63 (2013) 123–151. [arXiv:1301.2826](#), [doi:10.1146/annurev-nucl-102212-170540](#).
- [46] F. G. Gardim, F. Grassi, M. Luzum, J.-Y. Ollitrault, Mapping the hydrodynamic response to the initial geometry in heavy-ion collisions, *Phys. Rev. C* 85 (2012) 024908. [arXiv:1111.6538](#), [doi:10.1103/PhysRevC.85.024908](#).
- [47] A. Bilandzic, C. H. Christensen, K. Gulbrandsen, A. Hansen, Y. Zhou, Generic framework for anisotropic flow analyses with multiparticle azimuthal correlations, *Phys. Rev. C* 89 (2014) 064904. [arXiv:1312.3572](#), [doi:10.1103/PhysRevC.89.064904](#).
- [48] J. Adam, et al., Correlated event-by-event fluctuations of flow harmonics in Pb-Pb collisions at $\sqrt{s_{NN}} = 2.76$ TeV, *Phys. Rev. Lett.* 117 (2016) 182301. [arXiv:1604.07663](#), [doi:10.1103/PhysRevLett.117.182301](#).
- [49] Y. Zhou, Review of anisotropic flow correlations in ultrarelativistic heavy-ion collisions, *Adv. High Energy Phys.* 2016 (2016) 9365637. [arXiv:1607.05613](#), [doi:10.1155/2016/9365637](#).
- [50] Z. Qiu, U. Heinz, Hydrodynamic event-plane correlations in Pb+Pb collisions at $\sqrt{s} = 2.76$ ATeV, *Phys. Lett. B* 717 (2012) 261–265. [arXiv:1208.1200](#), [doi:10.1016/j.physletb.2012.09.030](#).

- [51] D. Teaney, L. Yan, Event-plane correlations and hydrodynamic simulations of heavy ion collisions, *Phys. Rev. C* 90 (2014) 024902. [arXiv:1312.3689](#), [doi:10.1103/PhysRevC.90.024902](#).
- [52] H. Niemi, K. J. Eskola, R. Paatelainen, Event-by-event fluctuations in a perturbative QCD + saturation + hydrodynamics model: Determining QCD matter shear viscosity in ultrarelativistic heavy-ion collisions, *Phys. Rev. C* 93 (2016) 024907. [arXiv:1505.02677](#), [doi:10.1103/PhysRevC.93.024907](#).
- [53] Y. Zhou, K. Xiao, Z. Feng, F. Liu, R. Snellings, Anisotropic distributions in a multiphase transport model, *Phys. Rev. C* 93 (2016) 034909. [arXiv:1508.03306](#), [doi:10.1103/PhysRevC.93.034909](#).
- [54] E. G. Judd, et al., The evolution of the STAR Trigger System, *Nucl. Instrum. Meth. A* 902 (2018) 228–237. [doi:10.1016/j.nima.2018.03.070](#).
- [55] M. Anderson, et al., The Star time projection chamber: A Unique tool for studying high multiplicity events at RHIC, *Nucl. Instrum. Meth. A* 499 (2003) 659–678. [arXiv:nucl-ex/0301015](#), [doi:10.1016/S0168-9002\(02\)01964-2](#).
- [56] B. Alver, M. Baker, C. Loizides, P. Steinberg, The PHOBOS Glauber Monte Carlo. [arXiv:0805.4411](#).
- [57] A. Bilandzic, R. Snellings, S. Voloshin, Flow analysis with cumulants: Direct calculations, *Phys. Rev. C* 83 (2011) 044913. [arXiv:1010.0233](#), [doi:10.1103/PhysRevC.83.044913](#).
- [58] K. Gajdošová, Investigations of anisotropic collectivity using multi-particle correlations in pp, p–Pb and Pb–Pb collisions, *Nucl. Phys. A* 967 (2017) 437–440. [doi:10.1016/j.nuclphysa.2017.04.033](#).
- [59] J. Jia, M. Zhou, A. Trzupek, Revealing long-range multiparticle collectivity in small collision systems via subevent cumulants, *Phys. Rev. C* 96 (2017) 034906. [arXiv:1701.03830](#), [doi:10.1103/PhysRevC.96.034906](#).
- [60] R. S. Bhalerao, J.-Y. Ollitrault, S. Pal, Event-plane correlators, *Phys. Rev. C* 88 (2013) 024909. [arXiv:1307.0980](#), [doi:10.1103/PhysRevC.88.024909](#).
- [61] N. Magdy, O. Evdokimov, R. A. Lacey, A method to test the coupling strength of the linear and nonlinear contributions to higher-order flow harmonics via Event Shape Engineering. [arXiv:2002.04583](#).
- [62] S. Acharya, et al., Linear and non-linear flow modes in Pb-Pb collisions at $\sqrt{s_{NN}} = 2.76$ TeV, *Phys. Lett. B* 773 (2017) 68–80. [arXiv:1705.04377](#), [doi:10.1016/j.physletb.2017.07.060](#).
- [63] P. Alba, V. Mantovani Sarti, J. Noronha, J. Noronha-Hostler, P. Parotto, I. Portillo Vazquez, C. Ratti, Effect of the QCD equation of state and strange hadronic resonances on multiparticle correlations in heavy ion collisions, *Phys. Rev. C* 98 (2018) 034909. [arXiv:1711.05207](#), [doi:10.1103/PhysRevC.98.034909](#).
- [64] B. Schenke, C. Shen, P. Tribedy, Multiparticle and charge-dependent azimuthal correlations in heavy-ion collisions at the Relativistic Heavy-Ion Collider, *Phys. Rev. C* 99 (2019) 044908. [arXiv:1901.04378](#), [doi:10.1103/PhysRevC.99.044908](#).